

Designing Selective Drug-like Molecular Glues for the  
Glucocorticoid Receptor/14-3-3 Protein–Protein InteractionJakob S. Pallesen,<sup>▽</sup> Claire C. Munier,<sup>▽</sup> Francesco Bosica, Sebastian A. Andrei, Karl Edman, Anders Gunnarsson, Giuseppina La Sala, Okky Dwichandra Putra, Sonja Srdanović, Andrew J. Wilson, Lisa Wissler, Christian Ottmann, Matthew W. D. Perry, and Gavin O'Mahony\*Cite This: *J. Med. Chem.* 2022, 65, 16818–16828

Read Online

ACCESS |



Metrics &amp; More



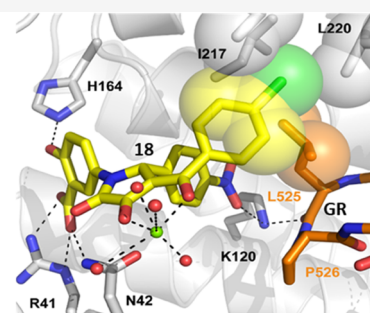
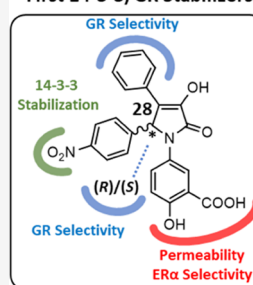
Article Recommendations



Supporting Information

**ABSTRACT:** The ubiquitously expressed glucocorticoid receptor (GR) is a nuclear receptor that controls a broad range of biological processes and is activated by steroidal glucocorticoids such as hydrocortisone or dexamethasone. Glucocorticoids are used to treat a wide variety of conditions, from inflammation to cancer but suffer from a range of side effects that motivate the search for safer GR modulators. GR is also regulated outside the steroid-binding site through protein–protein interactions (PPIs) with 14-3-3 adapter proteins. Manipulation of these PPIs will provide insights into noncanonical GR signaling as well as a new level of control over GR activity. We report the first molecular glues that selectively stabilize the 14-3-3/GR PPI using the related nuclear receptor estrogen receptor  $\alpha$  (ER $\alpha$ ) as a selectivity target to drive design. These 14-3-3/GR PPI stabilizers can be used to dissect noncanonical GR signaling and enable the development of novel atypical GR modulators.

## First 14-3-3/GR Stabilizers



## INTRODUCTION

Molecular glues, or protein–protein interaction (PPI) stabilizers, are compounds that interact at the interface between two proteins to induce or enhance the affinity of their PPI. Recently, there has been a surge of interest in molecular glues due to the discovery of the so-called glue degraders,<sup>1</sup> which are monofunctional compounds (unlike the bifunctional PROTACs)<sup>2</sup> that induce protein degradation by inducing a PPI between the protein to be degraded and an E3 ligase of the ubiquitin–proteasome system. Choosing a suitable “effector” protein platform other than E3 ligases could open up a range of pharmacological modes of action for molecular glues beyond degradation. The 14-3-3 proteins are a family of eukaryotic regulatory adapter proteins<sup>3</sup> that bind to and exert downstream effects (such as nuclear exclusion,<sup>4</sup> membrane localization,<sup>5</sup> or degradation)<sup>6</sup> on phosphoproteins and represent such a potential effector protein platform for molecular glues. Given that many 14-3-3 binding partners are classically undruggable proteins such as transcription factors or other intrinsically disordered proteins, molecular glues that stabilize 14-3-3 PPIs could represent small-molecule approaches to modulation of these targets.

A small number of molecular glues that stabilize 14-3-3 PPIs have been identified, with the most extensively studied being the natural product Fusicoccin A (FC-A).<sup>7</sup> FC-A stabilizes 14-3-3 PPIs by occupying a binding pocket (the “FC-A pocket”) at the PPI interface.<sup>7</sup> Small-molecule stabilizers of the 14-3-3/

estrogen receptor  $\alpha$  (ER $\alpha$ ) PPI, such as compound **1**, have also been shown to occupy the FC-A pocket.<sup>8</sup> 14-3-3 contributes a large proportion of the surface of the FC-A pocket, which is therefore conserved across many 14-3-3 PPIs; the structural diversity of the PPI interface pockets comes almost entirely from client protein structural diversity. Given that the client proteins bind via a relatively limited set of 14-3-3 consensus motifs, this raises the question as to how much selectivity can be achieved for a 14-3-3 molecular glue. Unlike PROTACs that can gain degradation selectivity for promiscuous warheads due to specificity within the ternary E3 ligase complex,<sup>9</sup> molecular glues need to be inherently specific for the PPI complex that they stabilize. We therefore set out to study the selectivity of molecular glues for 14-3-3 PPIs with the related nuclear receptor proteins glucocorticoid receptor (GR) and ER $\alpha$ .

GR is a ubiquitously expressed ligand-dependent transcription factor of the nuclear receptor class and regulates the expression of thousands of genes controlling a wide range of fundamental processes.<sup>10</sup> GR agonists are extensively used

Received: October 6, 2022

Published: December 9, 2022



Table 1. 14-3-3 $\zeta$ /GR and 14-3-3 $\zeta$ /ER $\alpha$  PPI Stabilization by Compounds 1, 17–30

#	R1	R2	R3	TE <sup>a</sup>		EC <sub>1,2</sub> ( $\mu$ M) <sup>b</sup>	
				GR	ER $\alpha$	GR	ER $\alpha$
1				1.4 $\pm$ 0.1	1.9 $\pm$ 0.1	63 (59-68)	28 (25-32)
(R)-1				1.6 $\pm$ 0.1	2.3 $\pm$ 0.2	32 (28-35)	15 (12-18)
(S)-1				1.2 $\pm$ 0.1	NS	162 (129-186)	NS
17				NS	NS	NS	NS
18				1.5 $\pm$ 0.1	2.1 $\pm$ 0.1	42 (36-47)	22 (18-26)
(R)-18				1.7 $\pm$ 0.1	1.6 $\pm$ 0.1	30 (21-40)	35 (26-47)
(S)-18				1.3 $\pm$ 0.1	NS	126 (98-166)	NS
19				NS	NS	NS	NS
20				1.2 $\pm$ 0.1	1.4 $\pm$ 0.2	96 (76-130)	73 (32-133)
21		Ph		NS	NS	NS	NS

<sup>a</sup>TE is the stabilization effect of a compound at 200  $\mu$ M and is the ratio of the signal obtained in the FP assays in the presence of the compound versus that obtained in the presence of DMSO. <sup>b</sup>EC<sub>1,2</sub> is the concentration of compound (in  $\mu$ M) that causes a 20% increase in assay signal of the 14-3-3–phosphopeptide complex. NS: No stabilization at the tested concentrations. Measurements were performed in triplicate, and the errors represent the standard deviation of the three independent experiments.

clinically for their powerful anti-inflammatory and immunosuppressive effects.<sup>11</sup> Canonical GR activation is via ligand

binding to the GR ligand binding domain (LBD), resulting in conformational changes, migration to the nucleus, and

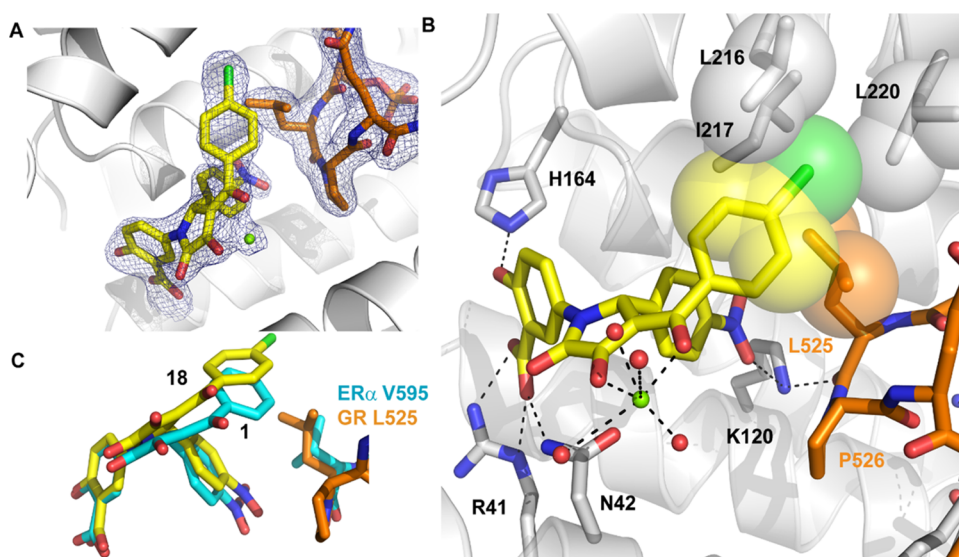


**Figure 1.** X-ray crystal structure of 14-3-3 $\zeta$ /GR\_pT524/(*R*)-18 (PDB 8A9G). 14-3-3 $\zeta$ : gray, GR\_pT524: orange sticks, and (*R*)-18: yellow sticks. (A) Ligand- and GR\_pT524-associated electron density ( $2F_{\text{obs}} - F_{\text{cal}}$  map contoured at  $1\sigma$ ); (B) details of interactions of (*R*)-18. The  $\text{Mg}^{2+}$  ion is shown as a green sphere, and water molecules as red spheres. (C) Comparison of ligand binding modes in 14-3-3 $\zeta$ /GR\_pT524/(*R*)-18 (yellow) and 14-3-3 $\sigma$ /ER $\alpha$ (pT594)/(*R*)-1 (PDB 6TJM, turquoise) ternary complexes.

modulation of gene transcription.<sup>12</sup> Noncanonically, GR is also regulated via 14-3-3 PPIs, with 14-3-3 being shown to interact with GR after phosphorylation of GR residue T524.<sup>13</sup> The 14-3-3/GR PPI is implicated in pathological inflammatory disorders and cancer,<sup>14,15</sup> and recently, GR was reported to inhibit cell proliferation through a nongenomic mechanism via 14-3-3-mediated RAS complexes.<sup>16</sup> An X-ray crystal structure of the binary complex between a phosphorylated 13-mer GR peptide (GR\_pT524) and 14-3-3 $\zeta$  identified a druggable pocket at the 14-3-3/GR interface, similar to the FC-A pocket in the 14-3-3/ER $\alpha$  complex.<sup>13</sup> It was hypothesized that ligands binding to this pocket would act as molecular glues that could be used to elucidate the pharmacological role of this PPI and aid in the development of novel atypical GR modulators.

Given that ER $\alpha$  and GR are both nuclear receptors of the NR3 family, the 14-3-3/ER $\alpha$ <sup>17,18</sup> and 14-3-3/GR PPIs also offered an opportunity to explore the design of molecular glue selectivity using two 14-3-3 client proteins from the same target class. In this paper, we report the first stabilizers of the 14-3-3/GR PPI. We also show that these compounds can be optimized to selectively stabilize the 14-3-3/GR PPI over the related 14-3-3/ER $\alpha$  PPI. The initial lead compounds had low cell permeability, and we also report stabilizers with improved cell permeability, thus enabling their use as early chemical tools for studying 14-3-3/GR PPI stabilization in cells.

## RESULTS AND DISCUSSION

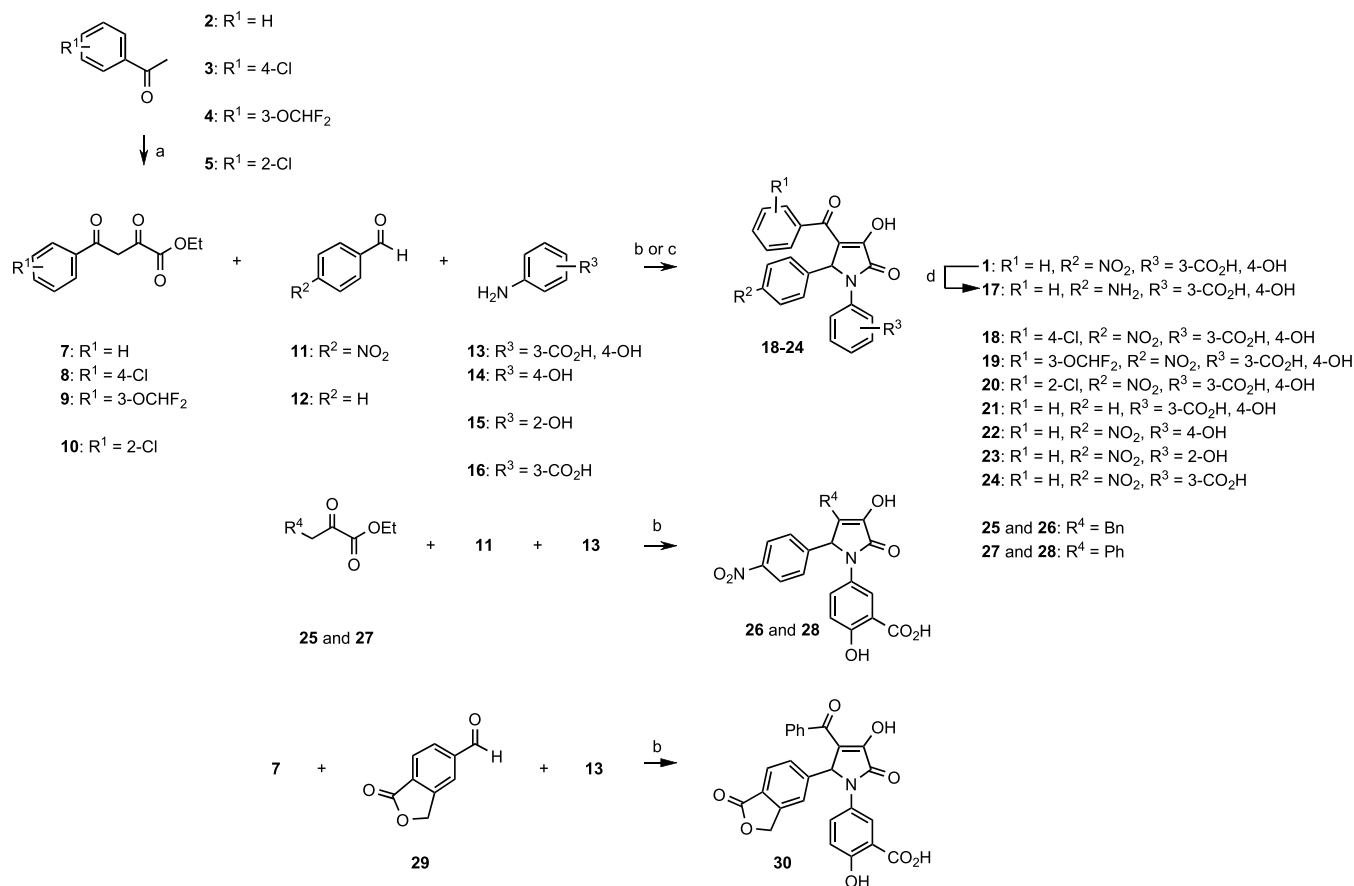
In spite of its use as the tool compound of choice in the field of 14-3-3 molecular glues, it has been reported that FC-A does not stabilize 14-3-3 PPIs with protein partners containing a proline at position +2 relative to the phosphorylated serine/threonine residue.<sup>19,20</sup> The GR pT524 site has a proline in the  $n + 2$  position (P526) (Figure S1); thus, the 14-3-3/GR PPI was expected to be insensitive to stabilization by FC-A. To investigate this experimentally, we developed fluorescence polarization (FP) and surface plasmon resonance (SPR) assays based on 14-3-3 $\zeta$  and GR\_pT524 and demonstrated that FC-A does not stabilize this PPI due to a steric clash between the

C12 hydroxy group of FC-A and P526 of GR (Figures S1 and S2).

Compound **1** is a stabilizer of the 14-3-3/ER $\alpha$  PPI and binds to the FC-A pocket of that binary complex.<sup>8</sup> As **1** was not expected to clash with GR P526 in 14-3-3/GR, its 14-3-3/GR PPI stabilization potency and efficacy were assessed using our FP assay. Compound **1** showed weak stabilization of the 14-3-3/GR PPI, with an incomplete concentration–response curve observed (Figure S3). To enable a comparison of compounds lacking full concentration–response curves, we derived the potency and efficacy parameters  $\text{EC}_{1,2}$ , the measure of concentration of compound which induces a 20% increase in assay signal, and Top Effect (TE) (see Table 1 for full definitions) from the FP assay curves. TE is, in effect, the fold stabilization of the PPI induced by the compound at the highest concentration tested compared to DMSO control and therefore is a measure of glue efficacy. The  $\text{EC}_{1,2}$  and TE of **1** for the 14-3-3/GR PPI were 63  $\mu\text{M}$  and 1.43 (Table 1), respectively, an approximately 2-fold decrease in potency compared to its activity for the 14-3-3/ER $\alpha$  PPI ( $\text{EC}_{1,2} = 28 \mu\text{M}$ , TE = 1.9). (*R*)-**1** was found to be the more active enantiomer in the 14-3-3/GR system, as previously reported for the 14-3-3/ER $\alpha$  PPI.<sup>8</sup> However, while (*S*)-**1** was completely inactive on the 14-3-3/ER $\alpha$  PPI, it unexpectedly showed weak stabilization of the 14-3-3/GR PPI ( $\text{EC}_{1,2} = 162 \mu\text{M}$ , TE = 1.2), making it a selective stabilizer of the 14-3-3/GR PPI. With the first confirmed stabilizers of the 14-3-3/GR PPI in hand, we set out to improve the 14-3-3/GR PPI stabilization potency and increase selectivity versus the 14-3-3/ER $\alpha$  PPI.

Initially, we used the X-ray crystal structure of (*R*)-**1**/14-3-3 $\sigma$ /ER $\alpha$  (PDB 6TJM)<sup>8</sup> to provide guidance on what features of (*R*)-**1** could be modified to improve stabilization potency and selectivity. The aryl moiety of (*R*)-**1** points toward the 14-3-3 binding partner (Figure 1B,C); thus, modifications here were expected to modulate 14-3-3 PPI stabilization selectivity. The nitro group of **1** accepts an H-bond from K122 of 14-3-3 $\sigma$ , so exploration of other H-bond-accepting moieties was desired. The salicylate carboxylate group makes a bidentate interaction

Scheme 1. Synthesis of compounds 1, 17–24, 26, 28, and 30



<sup>a</sup>Diethyl oxalate (6), EtONa, 16 h, 0 °C—RT, yield ND. <sup>b</sup>for 1, 18–22, 24, 26, 28, and 30: AcOH, 2 h, 120 °C, 2–60%. <sup>c</sup>for 23: AcOH, 3 days, RT, 39%. <sup>d</sup>5% Pd/C, H<sub>2</sub>, 1 atm, MeOH, 6 h, RT, 9%.

with 14-3-3σ R42, but together with the vinylogous carboxylate moiety, the charged functionality was expected to impair cell permeability, so we also explored modifications of this functionality.

The compounds were synthesized as shown in Scheme 1. Diketooesters 7–10 were synthesized by mixed Claisen condensations between the requisite acetophenones 2–5 and diethyl oxalate 6.<sup>21</sup> One-pot multicomponent condensations of diketooesters 7–10, aldehydes 11, 12 or 29, and anilines 13–16 afforded final compounds 18–24 and 30. Compounds 26 and 28 were synthesized similarly but from β-ketoesters 25 and 27, respectively. Compound 17 was obtained by catalytic hydrogenation of the nitro group of 1. The enantiomers of 18 and 28 were separated by chiral high-performance liquid chromatography (HPLC).

The 14-3-3/GR and 14-3-3/ERα PPI stabilization of compounds 17–24, 26, 28, and 30 was then assessed using our FP assays (Table 1 and Figure S3). Modifications of the aroyl moiety (R<sup>1</sup>) were expected to influence selectivity of 14-3-3 PPI stabilization. A 4-Cl on the R<sup>1</sup> phenyl ring (18) gave similar activity for both GR and ERα and a slight potency increase versus 1. Similarly to 1, (R)-18 was the more active enantiomer for both PPIs. (S)-18 showed weak, selective stabilization of the 14-3-3/GR complex (EC<sub>1,2</sub> = 126 μM, TE = 1.3). A 3-OCHF<sub>2</sub> on the R<sup>1</sup> phenyl (19) abolished activity for both GR and ERα, and a 2-Cl substituent (20) was tolerated but provided no improvement in activity compared to 1. Replacing the carbonyl of the vinylogous carboxylate with

a methylene afforded 26 (R<sup>1</sup> = Bn) and led to a significant decrease in 14-3-3/ERα potency (EC<sub>1,2</sub> = 175 μM, TE = 1.2) but only a moderate drop in 14-3-3/GR potency (EC<sub>1,2</sub> = 82 μM, TE = 1.3), making 26 a moderately 14-3-3/GR-selective stabilizer. Removing the methylene linker of 26 afforded 28 (R<sup>1</sup> = Ph). Compound 28 was inactive in the 14-3-3/ERα system and showed further improved 14-3-3/GR potency vs 26 (EC<sub>1,2</sub> = 45 μM, TE = 1.4). Comparing matched pair 28 (R<sup>1</sup> = Ph) and 1 (R<sup>1</sup> = CPh) shows that 14-3-3/GR PPI stabilization selectivity can be achieved. Chiral separation of 28 showed that only (–)-28 stabilized the 14-3-3/GR PPI (EC<sub>1,2</sub> = 40 μM, TE = 1.5) and no 14-3-3/ERα PPI stabilization activity for either (–)-28 or (+)-28.

Compound 18 was inactive in a GR binding assay (see the Supporting Information). Compound 18 was cocrystallized with 14-3-3ζ and GR\_pT524 (PDB 8A9G), and the structure solved to 1.96 Å resolution (Figure 1). (R)-18 was modeled into the observed ligand electron density (Figure 1A), in agreement with the FP data, which showed (R)-18 to be the more active enantiomer. As expected, 18 binds in a pocket overlapping with the FC-A pocket and is involved in a network of polar interactions, with 14-3-3 residue K120 simultaneously donating H-bonds to the backbone carbonyl of GR P526 and the nitro group of (R)-18. Also, similarly to our previous observations in the 14-3-3σ/ERα/(R)-1 ternary complex,<sup>8</sup> a fully hydrated Mg<sup>2+</sup> ion was observed to be chelated by the vinylogous carboxylate moiety of (R)-18, locking the conformation of the aroyl moiety into the preferred binding

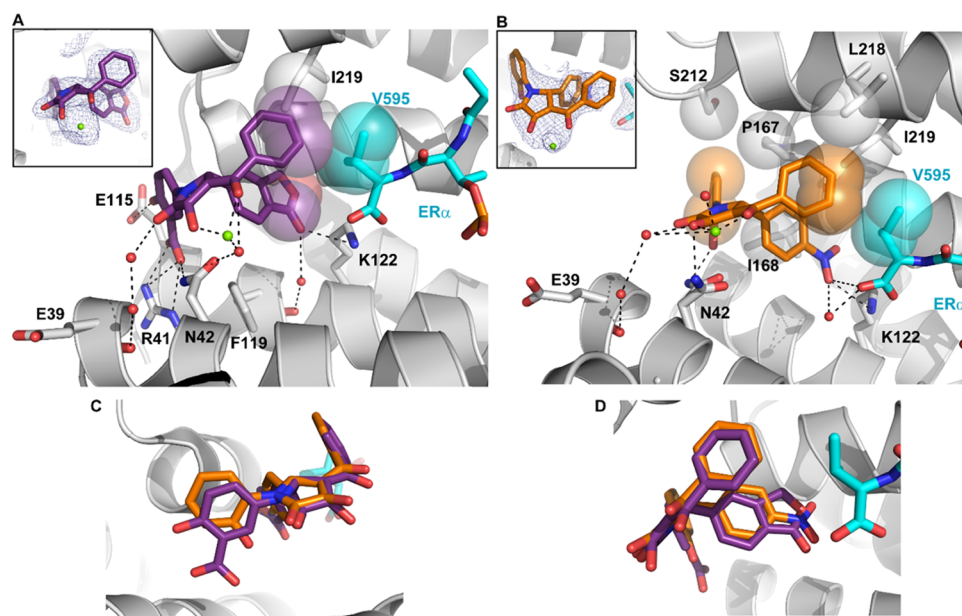


**Figure 2.** X-ray crystal structure of 14-3-3 $\sigma$ /ER $\alpha$ (pT594)/(R)-30 (PDB 7PWZ) and 14-3-3 $\sigma$ /ER $\alpha$ (pT594)/(R)-23 (PDB 7PWT). 14-3-3: gray, ER $\alpha$ \_pT594: turquoise sticks, (R)-30: purple sticks, and (R)-23: orange sticks. (A) Details of interactions of (R)-30 and ligand-associated electron density ( $2F_{\text{obs}} - F_{\text{cal}}$  map contoured at  $1\sigma$ ). (B) Details of interactions of (R)-23 and ligand-associated electron density ( $2F_{\text{obs}} - F_{\text{cal}}$  map contoured at  $1\sigma$ ). The Mg $^{2+}$  ion is shown as a green sphere, and water molecules as red spheres. (C, D) Comparison of binding mode of (R)-30 and (R)-23 centered around the salicylate moiety of (R)-30 (panel C) and the nitrophenyl moiety of (R)-23 (panel D).

conformation (Figure 1A,B). In the 14-3-3 $\zeta$ /GR/(R)-18 ternary complex, the hydroxyl of the salicylate moiety forms an H-bond to H164, whereas in the 14-3-3 $\sigma$ /ER $\alpha$ /(R)-1 ternary complex, the analogous hydroxyl forms an H-bond to 14-3-3 $\sigma$  E115. In addition, 14-3-3 residues L220, L216, and I217, and GR\_T524 residue L525 formed a hydrophobic sub-pocket, which accommodated the Cl substituent of (R)-18 (Figure 1B). (S)-18 could be modeled into the electron density of 14-3-3 $\zeta$ /GR/18 due to the pseudosymmetry of 18 around the pyrrolidone ring (Figure S4), but with a poorer fit. The binding mode of (S)-18 retained the H-bond between the nitro group and 14-3-3 $\zeta$  K120, but the salicylate and aryl moieties point in opposite directions compared to (R)-18, with a novel polar interaction between the salicylate carboxylate group of (S)-18 and GR Q527.

Overlay of 14-3-3/GR and 14-3-3/ER $\alpha$  complex crystal structures showed an equivalent hydrophobic sub-pocket in 14-3-3/ER $\alpha$ , partly lined by ER $\alpha$  V595 (Figure 1C). The 3-position of the R $^1$  aryl phenyl ring occupies a somewhat sterically congested region of the pocket, indicating that substitution would not be tolerated due to a steric clash with the phosphopeptides on one side and I217 of 14-3-3 on the other. This was confirmed by the inactivity of 3-OCHF $_2$  derivative 19. The larger GR L525 residue compared to ER $\alpha$  V595 causes a slight shift (approximately 2 Å) of the aryl moiety of 18 in the 14-3-3/GR complex relative to the position of 1 in the 14-3-3/ER $\alpha$  complex (Figure 1C). Replacing the R $^1$  aryl group with Bn (26) or Ph (28) led to reduced or no activity at 14-3-3/ER $\alpha$  and therefore selectivity toward 14-3-3/GR. In the case of 26, removal of the carbonyl prevents the conformational restriction afforded by metal chelation to the vinylogous carboxylate moiety and a likely mismatch between solution-phase and binding conformations of the ligand. ER $\alpha$  binds 14-3-3 at its C-terminus, while the 14-3-3 binding motif of GR is internal, resulting in the Ph of 28 being solvent-exposed in 14-3-3/ER $\alpha$  (therefore making no productive

interactions) but buried in a well-defined sub-pocket in 14-3-3/GR.

Interestingly, both (S)-1 and (S)-18 selectively stabilize the 14-3-3/GR PPI over 14-3-3/ER $\alpha$  (Table 1). Docking calculations show that the best-scored pose of (S)-1 in 14-3-3 $\zeta$ /GR matches with the refined model of 14-3-3 $\zeta$ /GR/(S)-18 (Figure S4), whereas in 14-3-3 $\zeta$ /ER $\alpha$ , (S)-1 assumes a new orientation where the nitro group points toward solvent (Figure S5), explaining its lack of activity in 14-3-3 $\zeta$ /ER $\alpha$ . The binding free energy of (R)-1 and (S)-1 in both 14-3-3 $\zeta$ /GR and 14-3-3 $\zeta$ /ER $\alpha$  complexes were estimated using the MD simulation-based molecular mechanics/generalized Born surface area (MMGBSA) method (see the Supporting Information and Figure S6). Similar binding energies were calculated for (R)-1 in 14-3-3 $\zeta$ /GR ( $\Delta G = -55.8 \pm 38.4$  kcal/mol) and 14-3-3 $\zeta$ /ER $\alpha$  ( $\Delta G = -44.9 \pm 25.3$  kcal/mol). However, (S)-1 showed less favorable binding energy with 14-3-3/ER $\alpha$  than 14-3-3/GR ( $\Delta G = -39.3 \pm 19.9$  and  $-69.9 \pm 30.7$  kcal/mol, respectively), supporting the 14-3-3/GR-selectivity of (S)-1 and, by extension, (S)-18. MD simulations on 14-3-3 $\zeta$ /GR/(S)-1 showed that the polar interaction between the nitro group and 14-3-3 $\zeta$  K120 was retained for  $\sim 95\%$  of the simulated time, and an additional polar interaction between the salicylate carboxylate group of (S)-1 and GR Q527 was formed (Figure S7). A similar interaction was impossible to obtain between (S)-1 and ER $\alpha$ .

For R $^2 = 4\text{-NO}_2\text{Ph}$ , the nitro group forms key polar interactions with 14-3-3 K120 and the GR P526 backbone carbonyl or ER $\alpha$  C-terminus. Nitro groups are excellent H-bond acceptors but are associated with mutagenicity and genotoxicity. Thus, an alternative group would be desirable to increase the drug-likeness of our compounds.<sup>22</sup> Removal (R $^2 = \text{Ph}$ , 21) or reduction to the corresponding aniline (R $^2 = 4\text{-NH}_2\text{Ph}$ , 17) led to a loss of measurable activity in both 14-3-3/GR and 14-3-3/ER $\alpha$  PPIs, consistent with the loss of an H-bond acceptor in this position. Benzolactone 30 retained

activity (GR:  $EC_{1,2} = 150 \mu\text{M}$ , TE = 1.2 and ER $\alpha$ :  $EC_{1,2} = 63 \mu\text{M}$ , TE = 1.6) and was selected for cocrystallization with 14-3-3 $\sigma$  and ER $\alpha$  pT594, resulting in a 2.50 Å X-ray crystal structure of 14-3-3/ER $\alpha$ /30 (PDB 7PWZ, Figure 2A). Only (R)-30 could be modeled into the observed electron density and, as expected, the lactone carbonyl moiety of 30 accepts an H-bond from 14-3-3 $\sigma$  K122 (analogous to K120 in 14-3-3 $\zeta$ , Figure 2A), effectively mimicking the nitro moiety.

R<sup>3</sup> modifications were also explored to probe the role of the salicylate moiety. As polar diacids, compounds 1, 17–21, 26, 28, and 30 were predicted in silico to have low cellular permeability,<sup>23</sup> making them unsuitable for development as chemical tools for use in cell assays. Therefore, less polar and/or uncharged salicylate replacements were sought. A Caco-2 permeability assay<sup>24</sup> confirmed low permeability for 1 ( $P_{\text{app}}$  (A to B) =  $0.047 \times 10^{-6}$  cm/s). X-ray crystal structures of 14-3-3/ER $\alpha$ /1 and 14-3-3/GR/18 ternary complexes (Figures 1B and 2A,B) showed a bidentate polar interaction between the salicylate carboxylate and the side chain of 14-3-3 R41, and loss of this interaction was expected to reduce activity. Removal of the salicylate carboxylate (R<sup>3</sup> = 4-OHPh, 22 and R<sup>3</sup> = 2-OHPh, 23) did not dramatically reduce the activity in the 14-3-3/ER $\alpha$  system (22:  $EC_{1,2} = 87 \mu\text{M}$ , TE = 1.6 and 23:  $EC_{1,2} = 75 \mu\text{M}$ , TE = 1.4). In addition, 22 and 23 also showed selectivity toward 14-3-3/ER $\alpha$ , both displaying only marginal activity at 14-3-3/GR (Table 1). This is surprising, as the R<sup>3</sup> group makes exclusive contact with 14-3-3 and does not interact with the 14-3-3 binding partner and would therefore not be expected to affect PPI stabilization selectivity. The mechanistic origins of this selectivity may be kinetic in nature and are currently under investigation and will be reported in due course. As expected, replacing the charged salicylate with an uncharged phenol increased the permeability of 22 and 23 by 3- and 5-fold, respectively, vs 1 (22:  $P_{\text{app}}$  (A to B) =  $0.13 \times 10^{-6}$  cm/s and 23:  $P_{\text{app}}$  (A to B) =  $0.25 \times 10^{-6}$  cm/s) and they are thus classified as medium permeability compounds. A 2.38 Å resolution X-ray crystal structure of the 14-3-3/ER $\alpha$  pT594/23 ternary complex was obtained by cocrystallization (PDB 7PWT, Figure 2B). As for 18 and 30, only (R)-23 could be modeled into the observed electron density (Figure 2B) and showed the OH group of the R<sup>3</sup> phenol making an H-bond interaction with the side chain of 14-3-3 R42. The unexpected activity of 23 suggests that the bidentate carboxylate-R41 interaction for R1 salicylates plays a lesser role in solution-phase binding events than suggested by crystallography, potentially due to kinetic and/or desolvation effects.

## CONCLUSIONS

In conclusion, we have identified the first 14-3-3/GR PPI stabilizers using pyrrolidone-based 14-3-3/ER $\alpha$  stabilizers as a starting point. We have also shown that the pyrrolidone chemotype can be modified to afford selective stabilizers of 14-3-3/GR over ER $\alpha$ , including (S)-1, (S)-18, and (–)-28, and demonstrated that selective 14-3-3 PPI stabilization is possible between closely related 14-3-3 binding partners from the same target class. We also report progress on structure-based design toward compounds with higher potency, such as 18, and improved properties. In particular, 23 is the first example of a pyrrolidone 14-3-3 PPI stabilizer with demonstrated cell permeability. These compounds are the first chemical tools that could be used to study the noncanonical regulation of GR activity to deliver future GR modulators with broad

applicability while avoiding issues from classical GR drugs interacting with GR LBD.

## EXPERIMENTAL SECTION

Additional experimental details, including general procedures, chiral separation and vibrational circular dichroism, fluorescence polarization, surface plasmon resonance and Caco-2 and GR binding assays, as well as supporting Tables S1 and S2 and Figures S1–S8 and spectroscopic data of products can be found in the Supporting Information. All compounds are >95% pure by HPLC analysis.

**Ethyl 2,4-dioxo-4-phenyl-butanoate.** <sup>1</sup>H NMR (400 MHz, CDCl<sub>3</sub>)  $\delta$  7.99 (d,  $J = 7.4$  Hz, 2H), 7.60 (t,  $J = 7.4$  Hz, 1H), 7.50 (t,  $J = 7.6$  Hz, 2H), 7.07 (s, 1H), 4.39 (q,  $J = 7.1$  Hz, 2H), 1.41 (t,  $J = 7.1$  Hz, 3H). <sup>13</sup>C NMR (101 MHz, CDCl<sub>3</sub>)  $\delta$  190.8, 169.9, 162.3, 135.0, 133.9, 129.0, 128.0, 98.1, 62.7, 14.2.

**5-(3-Benzoyl-4-hydroxy-2-(4-nitrophenyl)-5-oxo-2,5-dihydro-1H-pyrrol-1-yl)-2-hydroxybenzoic Acid (1).** <sup>1</sup>H NMR (400 MHz, DMSO)  $\delta$  7.97–8.18 (m, 3H), 7.66–7.77 (m, 5H), 7.52–7.61 (m, 1H), 7.45 (t,  $J = 7.6$  Hz, 2H), 6.91 (d,  $J = 8.9$  Hz, 1H), 6.46 (s, 1H). <sup>13</sup>C NMR (101 MHz, DMSO)  $\delta$  189.0, 171.2, 164.5, 158.8, 151.0, 147.2, 144.4, 137.9, 132.7, 130.6, 129.3, 128.7, 128.2, 127.5, 124.9, 123.5, 119.1, 117.6, 113.0, 60.8. High-resolution mass spectrometry (HRMS) (ESI)  $m/z$  [M + H]<sup>+</sup> calcd for C<sub>24</sub>H<sub>16</sub>N<sub>2</sub>O<sub>8</sub>: 461.0985, found: 461.0974.

**5-(2-(4-Aminophenyl)-3-benzoyl-4-hydroxy-5-oxo-2,5-dihydro-1H-pyrrol-1-yl)-2-hydroxybenzoic Acid (17).** In a round-bottom flask, 1 (100 mg, 0.22 mmol) and Pd/C 5% (45 mg, 0.011 mmol) were suspended in MeOH (5 mL). The reaction was allowed to stir at room temperature (RT) under an atmosphere of H<sub>2</sub> (1 bar) until complete consumption of starting material (6 h). The catalyst was removed by filtration through a plug of celite, the filtrate was concentrated under vacuum, and the resulting solid was purified by preparative HPLC (S–95% ACN in 0.1 M FA, flow rate 60 mL/min). The collected fractions were freeze-dried to give compound 17 (8 mg, 9%) as an off-white solid. <sup>1</sup>H NMR (500 MHz, DMSO) 6.02 (s, 1H), 6.32–6.38 (m, 2H), 6.87 (d,  $J = 8.9$  Hz, 1H), 6.92–6.97 (m, 2H), 7.46 (t,  $J = 7.7$  Hz, 2H), 7.54–7.59 (m, 1H), 7.61 (dd,  $J = 8.9, 2.7$  Hz, 1H), 7.69–7.75 (m, 2H), 7.94 (d,  $J = 2.7$  Hz, 1H). <sup>13</sup>C NMR (126 MHz, DMSO)  $\delta$  189.5, 171.3, 164.3, 158.7, 148.0, 137.9, 132.7, 130.5, 128.8, 128.3, 128.2, 127.8, 124.9, 122.4, 120.3, 117.2, 113.9, 104.6, 61.7. HRMS (ESI)  $m/z$  [M + H]<sup>+</sup> calcd for C<sub>24</sub>H<sub>18</sub>N<sub>2</sub>O<sub>6</sub>: 431.1243, found: 431.1245. Purity: 97%.

**General Procedure for the Synthesis of Compounds 18–22, 24, 26, 28, and 30.** In a 20 mL vial, to a solution of diketooesters in AcOH, aldehyde and aniline were added. The vial was capped and heated at 120 °C for 180 min in a single-node microwave reactor. The pressure monitored was 1 bar.

**5-(3-(4-Chlorobenzoyl)-4-hydroxy-2-(4-nitrophenyl)-5-oxo-2,5-dihydro-1H-pyrrol-1-yl)-2-hydroxybenzoic Acid (18).** The compound was prepared from methyl 4-(4-chlorophenyl)-2,4-dioxobutanoate (150 mg, 0.62 mmol) in AcOH (5 mL), 4-nitrobenzaldehyde (96 mg, 0.62 mmol), and 5-amino-2-hydroxybenzoic acid (100 mg, 0.62 mmol). The mixture was diluted with diethyl ether and filtered. The solid residue was washed with diethyl ether and dried under reduced pressure to give compound 18 (60 mg, 20%) as a yellow solid. <sup>1</sup>H NMR (400 MHz, DMSO)  $\delta$  8–8.11 (m, 3H), 7.65–7.77 (m, 5H), 7.48–7.57 (m, 2H), 6.91 (d,  $J = 8.9$  Hz, 1H), 6.44 (s, 1H). <sup>13</sup>C NMR (101 MHz, DMSO)  $\delta$  187.8, 171.1, 164.3, 158.8, 151.7, 147.2, 144.4, 137.5, 136.6, 130.6, 129.3, 128.3, 127.4, 124.9, 123.5, 118.7, 117.6, 113.0, 60.8. HRMS (ESI)  $m/z$  [M + H]<sup>+</sup> calcd for C<sub>24</sub>H<sub>15</sub>ClN<sub>2</sub>O<sub>8</sub>: 495.0595, found: 495.0577.

**5-(3-(3-(Difluoromethoxy)benzoyl)-4-hydroxy-2-(4-nitrophenyl)-5-oxo-2,5-dihydro-1H-pyrrol-1-yl)-2-hydroxybenzoic Acid (19).** The compound was prepared from methyl 4-(3-(difluoromethoxy)phenyl)-2,4-dioxobutanoate (120 mg, 0.44 mmol) in AcOH (5 mL), 4-nitrobenzaldehyde (68.0 mg, 0.44 mmol), and 5-amino-2-hydroxybenzoic acid (71.1 mg, 0.44 mmol). After solvent removal, the crude product was purified by preparative HPLC (S–95% ACN with 0.2% NH<sub>3</sub>, flow rate 60 mL/min). The collected fractions were freeze-dried to give compound 19 (42 mg, 18%) as a pale yellow solid. <sup>1</sup>H

NMR (600 MHz, DMSO) 6.06 (s, 1H), 6.63 (d,  $J = 8.7$  Hz, 1H), 7.08 (s, 1H), 7.20 (d,  $J = 3.2$  Hz, 1H), 7.37 (t,  $J = 7.9$  Hz, 1H), 7.41–7.46 (m, 1H), 7.53–7.61 (m, 3H), 7.64 (d,  $J = 7.8$  Hz, 1H), 7.87 (d,  $J = 2.8$  Hz, 1H), 8–8.06 (m, 2H).  $^{13}\text{C}$  NMR (126 MHz, DMSO)  $\delta$  188.62, 171.19, 163.11, 159.24, 150.40 ( $J = 3.3$ ), 146.98, 146.71, 145.38, 141.30, 129.32, 129.05, 128.96, 127.28, 125.50, 124.73, 123.31, 123.20, 121.37, 118.67, 118.50, 116.93, 116.46, 114.41, 60.82. HRMS (ESI)  $m/z$  [ $M + H$ ] $^+$  calcd for  $\text{C}_{25}\text{H}_{16}\text{F}_2\text{N}_2\text{O}_9$ : 527.0902, found: 527.0887. Purity: 96%.

**5-(3-(2-Chlorobenzoyl)-4-hydroxy-2-(4-nitrophenyl)-5-oxo-2,5-dihydro-1H-pyrrol-1-yl)-2-hydroxybenzoic Acid (20).** The compound was prepared from methyl 4-(2-chlorophenyl)-2,4-dioxobutanoate (130 mg, 0.54 mmol) in AcOH (5 mL), 4-nitrobenzaldehyde (83 mg, 0.54 mmol), and 5-amino-2-hydroxybenzoic acid (87 mg, 0.54 mmol). After solvent removal, the crude product was purified by preparative HPLC (5–95% ACN with 0.1 M FA, flow rate 60 mL/min). The collected fractions were freeze-dried to give compound **20** (99 mg, 37%) as an off-white solid.  $^1\text{H}$  NMR (600 MHz, DMSO)  $\delta$  8.10 (d,  $J = 8.8$  Hz, 2H), 7.99 (d,  $J = 2.7$  Hz, 1H), 7.61–7.71 (m, 3H), 7.39–7.49 (m, 2H), 7.33–7.39 (m, 1H), 7.27 (d,  $J = 7.2$  Hz, 1H), 6.87 (d,  $J = 8.9$  Hz, 1H), 6.36 (s, 1H).  $^{13}\text{C}$  NMR (126 MHz, DMSO)  $\delta$  171.19, 164.44, 158.96, 147.13, 144.90, 139.75, 131.11, 130.47, 129.61, 129.43, 129.38, 128.45, 127.32, 127.16, 125.05, 123.42, 117.56, 113.27, 60.24. HRMS (ESI)  $m/z$  [ $M + H$ ] $^+$  calcd for  $\text{C}_{24}\text{H}_{15}\text{ClN}_2\text{O}_8$ : 495.0595, found: 495.0583. Purity: 99%.

**5-(3-Benzoyl-4-hydroxy-5-oxo-2-phenyl-2,5-dihydro-1H-pyrrol-1-yl)-2-hydroxybenzoic Acid (21).** The compound was prepared from ethyl 2,4-dioxo-4-phenylbutanoate (300 mg, 1.36 mmol), benzaldehyde (0.138 mL, 1.36 mmol), and 5-amino-2-hydroxybenzoic acid (209 mg, 1.36 mmol). After solvent removal, the reaction mixture was triturated with diethyl ether. The solid residue was washed with diethyl ether and subsequently purified by preparative HPLC (2–94% ACN in 0.2%  $\text{NH}_3$ , flow rate 60 mL/min). The collected fractions were freeze-dried to give the title compound **21** (124 mg, 22%) as an off-white solid.  $^1\text{H}$  NMR (400 MHz, DMSO) 6.25 (s, 1H), 6.89 (d,  $J = 8.9$  Hz, 1H), 7.07–7.16 (m, 1H), 7.16–7.25 (m, 2H), 7.31–7.4 (m, 2H), 7.45 (t,  $J = 7.7$  Hz, 2H), 7.53–7.58 (m, 1H), 7.64–7.75 (m, 3H), 7.99 (d,  $J = 2.7$  Hz, 1H), 11.83 (s, 1H).  $^{13}\text{C}$  NMR (101 MHz, DMSO)  $\delta$  189.24, 171.25, 164.45, 158.62, 150.06, 137.88, 136.23, 132.70, 130.68, 128.76, 128.41, 128.21, 128.02, 127.81, 127.72, 124.84, 120.01, 117.37, 112.86, 61.71. HRMS (ESI)  $m/z$  [ $M + H$ ] $^+$  calcd for  $\text{C}_{24}\text{H}_{17}\text{NO}_6$ : 415.1134, found: 415.1127. Purity: 95%.

**4-Benzoyl-3-hydroxy-1-(4-hydroxyphenyl)-5-(4-nitrophenyl)-1,5-dihydro-2H-pyrrol-2-one (22).** The compound was prepared from ethyl 2,4-dioxo-4-phenylbutanoate (480 mg, 2.18 mmol) in AcOH (8 mL), 4-nitrobenzaldehyde (329 mg, 2.18 mmol), and 4-aminophenol (238 mg, 2.18 mmol). After solvent removal, the crude product was purified by preparative HPLC (25–65% ACN  $\text{H}_2\text{O}/\text{ACN}/\text{FA}$  95/5/0.2 buffer over 20 min, with a flow of 100 mL/min). The collected fractions were freeze-dried to give compound **22** (48 mg, 5%) as an off-white solid.  $^1\text{H}$  NMR (500 MHz, DMSO)  $\delta$  12.13 (br, 1H), 9.48 (s, 1H), 8.02–8.08 (m, 2H), 7.69–7.73 (m, 2H), 7.64–7.69 (m, 2H), 7.53–7.59 (m, 1H), 7.44 (t,  $J = 7.7$  Hz, 2H), 7.34–7.4 (m, 2H), 6.65–6.7 (m, 2H), 6.36 (s, 1H).  $^{13}\text{C}$  NMR (126 MHz, DMSO)  $\delta$  189.0, 164.3, 163.1, 155.4, 147.1, 144.9, 138.0, 132.6, 129.3, 128.7, 128.2, 127.5, 124.7, 123.4, 118.7, 115.3, 60.9. HRMS (ESI)  $m/z$  [ $M + H$ ] $^+$  calcd for  $\text{C}_{23}\text{H}_{16}\text{N}_2\text{O}_6$ : 417.1086, found: 417.1089. Purity: 99%.

**4-Benzoyl-3-hydroxy-1-(2-hydroxyphenyl)-5-(4-nitrophenyl)-1,5-dihydro-2H-pyrrol-2-one (23).** In an round bottomed flask, to a solution of ethyl 2,4-dioxo-4-phenylbutanoate (1000 mg, 4.54 mmol) in AcOH (20 mL), 4-nitrobenzaldehyde (686 mg, 4.54 mmol) and 2-aminophenol (496 mg, 4.54 mmol) were added. The reaction mixture was stirred at RT for 3 days. After filtration, the solid residue was purified by preparative HPLC (25–65% ACN in  $\text{H}_2\text{O}/\text{ACN}/\text{FA}$  95/5/0.2 over 20 min, flow rate of 100 mL/min). The collected fractions were freeze-dried to give compound **23** (743 mg, 39%) as a white solid.  $^1\text{H}$  NMR (500 MHz, DMSO)  $\delta$  = 10.00 (s, 1H), 8.01–8.07 (m, 2H), 7.71–7.77 (m, 2H), 7.61–7.67 (m, 2H), 7.54–7.61 (m, 1H), 7.42–7.5 (m, 2H), 7.14 (dd,  $J = 7.9, 1.7$ , 1H), 7.06 (ddd,  $J = 8.2, 7.3, 1.7$ , 1H), 6.86 (dd,  $J = 8.1, 1.4$ , 1H), 6.72 (td,  $J = 7.6, 1.4$ , 1H), 6.24

(s, 1H).  $^{13}\text{C}$  NMR (126 MHz, DMSO)  $\delta$  189.3, 164.7, 152.9, 151.8, 147.3, 144.5, 137.9, 132.8, 129.4, 128.9, 128.9, 128.9, 128.8, 128.3, 123.5, 122.5, 119.2, 119.2, 118.2, 116.7, 61.6. HRMS (ESI)  $m/z$  [ $M + H$ ] $^+$  calcd for  $\text{C}_{23}\text{H}_{16}\text{N}_2\text{O}_6$ : 417.1086, found: 417.1079. Purity: 95%.

**3-(3-Benzoyl-4-hydroxy-2-(4-nitrophenyl)-5-oxo-2,5-dihydro-1H-pyrrol-1-yl)benzoic Acid (24).** The compound was prepared from ethyl 2,4-dioxo-4-phenylbutanoate (200 mg, 0.91 mmol) in AcOH (7 mL), 4-nitrobenzaldehyde (137 mg, 0.91 mmol), and 3-aminobenzoic acid (125 mg, 0.91 mmol). After solvent removal, the reaction mixture was triturated with diethyl ether. The solid residue was washed with diethyl ether and subsequently purified by preparative HPLC (5–95% ACN in 0.2%  $\text{NH}_3$ , flow rate 60 mL/min). The collected fractions were freeze-dried to give compound **24** (90 mg, 22%) as a pale yellow solid.  $^1\text{H}$  NMR (600 MHz, DMSO)  $\delta$  13.01 (br, 1H), 8.32–8.38 (m, 1H), 8.03 (d,  $J = 8.9$  Hz, 2H), 7.78–7.84 (m, 1H), 7.73–7.78 (m, 2H), 7.65 (d,  $J = 8.8$  Hz, 2H), 7.62 (d,  $J = 7.8$  Hz, 1H), 7.38–7.43 (m, 2H), 7.33 (t,  $J = 7.6$  Hz, 2H), 7.18 (br, 3H), 6.29 (s, 1H).  $^{13}\text{C}$  NMR (126 MHz, DMSO)  $\delta$  185.4, 168.9, 167.0, 149.1, 146.4, 140.4, 137.6, 131.3, 130.2, 129.0, 128.8, 128.7, 127.1, 125.4, 125.3, 123.0, 122.6, 60.1. HRMS (ESI)  $m/z$  [ $M + H$ ] $^+$  calcd for  $\text{C}_{24}\text{H}_{16}\text{N}_2\text{O}_7$ : 445.1036, found: 445.1025. Purity: 98%.

**5-(3-Benzoyl-4-hydroxy-2-(4-nitrophenyl)-5-oxo-2,5-dihydro-1H-pyrrol-1-yl)-2-hydroxybenzoic Acid (26).** The compound was prepared from ethyl 2-oxo-4-phenylbutanoate (250 mg, 1.21 mmol), 4-nitrobenzaldehyde (183 mg, 1.21 mmol), and 5-amino-2-hydroxybenzoic acid (186 mg, 1.21 mmol). After solvent removal, the crude mixture was purified by preparative SFC (MeOH/ $\text{NH}_3$  20 mM). The collected fractions were dried under reduced pressure to give compound **26** (10 mg, 2%) as a pale yellow solid.  $^1\text{H}$  NMR (500 MHz, DMSO) 3.07 (d,  $J = 15.0$  Hz, 1H), 3.70 (d,  $J = 15.0$  Hz, 1H), 5.63 (s, 1H), 6.65 (t,  $J = 7.7$  Hz, 1H), 6.78 (d,  $J = 8.1$  Hz, 1H), 6.93–7.08 (m, 4H), 7.1–7.23 (m, 3H), 7.34 (d,  $J = 8.2$  Hz, 2H), 8.02 (d,  $J = 8.1$  Hz, 2H), 9.73 (s, 1H), 9.94 (s, 1H).  $^{13}\text{C}$  NMR (151 MHz, DMSO, 25 °C)  $\delta$  166.14, 152.66, 147.14, 144.54, 143.27, 138.58, 129.11, 128.97, 128.45, 128.31, 128.04, 126.07, 124.47, 123.58, 123.47, 118.95, 118.08, 116.48, 62.81, 29.79. HRMS (ESI)  $m/z$  [ $M + H$ ] $^+$  calcd for  $\text{C}_{24}\text{H}_{18}\text{N}_2\text{O}_7$ : 447.1192, found: 447.1169. Purity: 96%.

**2-Hydroxy-5-(3-hydroxy-5-(4-nitrophenyl)-2-oxo-4-phenyl-2,5-dihydro-1H-pyrrol-1-yl)benzoic Acid (28).** The compound was prepared from ethyl 2-oxo-4-phenylpropanoate (150 mg, 0.78 mmol), 4-nitrobenzaldehyde (118 mg, 0.78 mmol), and 5-amino-2-hydroxybenzoic acid (120 mg, 0.78 mmol). After solvent removal, the crude mixture was purified to give compound **28** (201 mg, 60%) as a gray solid.  $^1\text{H}$  NMR (500 MHz, DMSO)  $\delta$  10.78 (s, 1H, OH), 8.08–8.04 (m, 2H, Ar), 8.00 (d,  $J = 2.7$  Hz, 1H, Ar), 7.72–7.69 (m, 3H, Ar), 7.67–7.62 (m, 2H, Ar), 7.31 (t,  $J = 7.8$  Hz, 2H, Ar), 7.21–7.15 (m, 1H, Ar), 6.91 (d,  $J = 9.0$  Hz, 1H, Ar), 6.71 (s, 1H, CH).  $^{13}\text{C}$  NMR (126 MHz, DMSO)  $\delta$  171.2, 165.1, 147.2, 145.4, 143.5, 131.1, 129.9, 129.0, 128.4, 127.5, 127.2, 124.1, 123.7, 121.8, 117.5, 60.7. HRMS (ESI)  $m/z$  [ $M + H$ ] $^+$  calcd ( $\text{C}_{23}\text{H}_{16}\text{N}_2\text{O}_7$ ): 433.1036, found: 433.1027. Purity: 95%.

**5-(3-Benzoyl-4-hydroxy-5-oxo-2-(1-oxo-1,3-dihydroisobenzofuran-5-yl)-2,5-dihydro-1H-pyrrol-1-yl)-2-hydroxybenzoic Acid (30).** The compound was prepared from ethyl 2,4-dioxo-4-phenylbutanoate (250 mg, 1.14 mmol), 1-oxo-1,3-dihydroisobenzofuran-5-carbaldehyde (185 mg, 1.14 mmol), and 5-amino-2-hydroxybenzoic acid (174 mg, 1.14 mmol). After solvent removal, the reaction mixture was triturated with diethyl ether. The solid residue was washed with diethyl ether and subsequently purified by preparative HPLC (5–95% ACN in 0.1 M FA, flow rate 60 mL/min). The collected fractions were freeze-dried to give compound **30** (192 mg, 35%) as a yellow solid.  $^1\text{H}$  NMR (500 MHz, DMSO) 5.28 (s, 2H), 6.42 (s, 1H), 6.86 (d,  $J = 8.9$  Hz, 1H), 7.44 (t,  $J = 7.7$  Hz, 2H), 7.53–7.59 (m, 1H), 7.62 (d,  $J = 8.0$  Hz, 1H), 7.65 (dd,  $J = 8.9, 2.7$  Hz, 1H), 7.67–7.75 (m, 4H), 8.02 (d,  $J = 2.8$  Hz, 1H).  $^{13}\text{C}$  NMR (126 MHz, DMSO)  $\delta$  188.9, 171.2, 170.0, 164.7, 159.0, 147.6, 143.8, 138.0, 132.6, 130.2, 128.9, 128.8, 128.2, 127.3, 125.0, 124.9, 124.9, 122.4, 119.2, 117.4, 69.7, 67.0, 61.4. HRMS (ESI)  $m/z$  [ $M + H$ ] $^+$  calcd for  $\text{C}_{26}\text{H}_{17}\text{NO}_8$ : 472.1032, found: 472.1045. Purity: 97%.

**Chiral Separation of 18:** (–) and (+)-5-(3-(4-Chlorobenzoyl)-4-hydroxy-2-(4-nitrophenyl)-5-oxo-2,5-dihydro-1H-pyrrol-1-yl)-2-hydroxybenzoic Acid ((–)-18 and (+)-18). The enantiomers of *rac*-18 (60 mg, 0.12 mmol) were separated by chiral column chromatography on a Chiralpak IC (250 mm × 20 mm, 5 μm) column. A solution of 18 (20 mg/mL in MeOH/IPA 2:1 + TEA) was injected and eluted with SFC MeOH/IPA/TEA 25:75:0.1 in CO<sub>2</sub>, 40 °C, a flow rate of 13 mL/min, and detected at 270 nm. The first eluted compound was collected and evaporated to afford (–)-18 (13 mg, 96% ee) as a yellow solid.  $[\alpha]_D^{20}$ : –23.2 (10 mg/mL, ACN/MeOH 1:1). The second eluted compound was collected and evaporated to afford (+)-18 (12 mg, 98% ee) as a yellow solid.  $[\alpha]_D^{20}$ : +18.8 (10 mg/mL, ACN/MeOH 1:1).

**Chiral Separation of 28.** The enantiomers of *rac*-28 were separated by chiral column chromatography on a Chiralpak IH (250 mm × 30 mm, 5 μm) column. A solution of 28 (34 mg/mL in DCM/MeOH 1:1) was injected and eluted with SFC 20% MeOH/MSA 100/20 mM in CO<sub>2</sub>, 25 °C, a flow rate of 150 mL/min, and detected at 210 nm. The first eluted compound was collected and evaporated to afford (–)-28 (71 mg, 99.4% ee) as a yellow solid.  $[\alpha]_D^{20}$ : –276 (10 mg/mL, ACN/MeOH 1:1). The second eluted compound was collected and evaporated to afford (+)-28 (95 mg, 96.8% ee) as a yellow solid.  $[\alpha]_D^{20}$ : +263 (10 mg/mL, ACN/MeOH 1:1).

**Vibrational Circular Dichroism Analysis of 18.** Vibrational circular dichroism (VCD) analysis was performed on (+)-18 only. The data collected suggest that (+)-18 is likely to be the (S) enantiomer. All spectra, experimental and simulated, are shown in the Supporting Information. (–)-18 (5.0 mg) and (+)-18 (5.4 mg) were dissolved in 150 μL of DMSO-*d*<sub>6</sub>, respectively. Approximately 90 μL of each solution was transferred to a 0.100 mm BaF<sub>2</sub> cell, and VCD spectra were acquired for 12 h in a Biotools ChiralIR-2X instrument. The resolution was 4 cm<sup>–1</sup>. The same cell was used for the measurement of both samples. A Monte Carlo molecular mechanics search for low-energy geometries was conducted for the S enantiomer of an analogue of this compound, with Cl replaced by H. MacroModel within the Maestro graphical interface (Schrödinger Inc.) was used to generate 123 starting coordinates for conformers. All conformers within 5 kcal/mol of the lowest energy conformer were used as starting points for density functional theory (DFT) minimizations within Gaussian09. Optimized structures, harmonic vibrational frequencies/intensities, VCD rotational strengths, and free energies at STP (including zero-point energies) were determined at B3LYP/6-31G\* level of theory. Three conformations were found that contributed over 10% to the Boltzmann distribution. An in-house program was used to fit Lorentzian line shapes (12 cm<sup>–1</sup> line width) to the computed spectrum of a Boltzmann distributed average, thereby allowing direct comparisons between simulated and experimental spectra.

**Crystal Data and Experimental Data for 28.** Single crystals of 28 were grown by solvent evaporation method using acetonitrile solvent. A suitable single crystal was mounted on an XtaLab Synergy-S diffractometer (Rigaku, Japan) equipped with a HyPix-Arc 100 curve detector (Rigaku, Japan) and an Oxford Cryosystems Cobra (Oxford Cryosystem, U.K.). Data were measured using Cu Kα radiation generated from a microfocus sealed tube (50 kV, 1 mA). Measurement strategy was calculated using CrysAlisPro software 1.171.42.35a.<sup>25</sup> Data reduction and correction were performed using CrysAlisPro software.<sup>8</sup> The structure was solved with ShelXT<sup>26</sup> structure solution program using the direct methods solution method within Olex2.<sup>27</sup> The model was refined on F<sub>o</sub><sup>2</sup> with ShelXL 2014.<sup>28</sup> All non-hydrogen atoms were refined anisotropically. All hydrogen atoms attached to oxygen atoms were located from the differential Fourier map and were refined isotropically. All other hydrogen atoms were determined geometrically and refined isotropically. CCDC 2190057 contains the supplementary crystallographic data for this paper. These data can be obtained free of charge via [www.ccdc.cam.ac.uk/data\\_request/cif](http://www.ccdc.cam.ac.uk/data_request/cif), by emailing [data\\_request@ccdc.cam.ac.uk](mailto:data_request@ccdc.cam.ac.uk), or by contacting the Cambridge Crystallographic Data Centre, 12 Union Road, Cambridge CB2 1EZ, UK; fax: +44 1223 336033. The

crystallographic data of 28 and the figure displaying the thermal ellipsoids can be found in the supporting information (Table S2 and Figure S8)

**Peptide Synthesis and Characterization.** Peptides were synthesized and purified, as described by Bosica et al.<sup>8</sup> and Munier et al.<sup>13</sup> Free N-terminus ERα\_pT594 for crystallization was purchased from Chinese Peptide Company.

**14-3-3 Protein Expression and Purification.** Proteins were expressed and purified as previously reported.<sup>8,13</sup>

**X-ray Crystallography. Cocrystallization of 14-3-3ζ, GR\_pT524, and 18.** Crystals were grown using the hanging drop vapor diffusion crystallization method by mixing 14-3-3ζΔC with GR\_pT524 in a 1:2 ratio, with a resulting protein concentration of 10 mg/mL in a crystallization buffer containing 20 mM HEPES pH 7.5, 2 mM MgCl<sub>2</sub> and 2 mM DTT. Compound 18 (2 mM) was added to the mixture, and after overnight incubation at 4 °C, hanging drops were formed by mixing equal volumes of protein/peptide/ligand solution and precipitant (0.4 M MgCl<sub>2</sub>, 27% PEG 3350, 0.1 M Bis Tris pH 6.5) (2 × 1 mL) on a 15-well EasyXtal (Qiagen) and equilibrated over a 500 μL reservoir at 4 °C. Crystals were harvested after 13 days, soaked in cryoprotectant containing the precipitant supplemented with 20% v/v glycerol, and flash-cooled in liquid nitrogen before data collection. Data collection and processing: Diffraction data were collected at the Swiss Light Source (SLS) in Switzerland (1.00003 Å, 100 K, SLS Beamline X06SA). Molecular replacement was performed using Phaser from the ccp4i package, and refinement and manual rebuilding was done using Buster and Coot software packages. The structure (PDB code: 8A9G) was refined to a resolution of 1.96 Å with Rwork/Rfree factors of 0.235/0.254. X-ray diffraction data collection and structure refinement statistics are summarized in Table S1. The figures were made using software PyMol (DeLano Scientific LLC).

**Cocrystallization of 14-3-3σ, ERα\_pT594, 23, and 30.** Crystals were grown by mixing 12.5 mg/mL 14-3-3σΔC with ERα\_pT594 in a molar ratio of 1:2 in 10 mM HEPES, pH 7.4, 150 mM NaCl, 2 mM BME, and 2 mM of the compound of interest and incubating overnight at 4 °C. The formed complex was then set up for crystallization by mixing 1:1 v/v 0.1 M Tris, pH 7.0, 0.2 M magnesium chloride hexahydrate, and 10% v/v PEG 8000 and incubating in a sitting drop at 4 °C. Crystals grew within a week and were cryoprotected by adding a grain of sucrose to the crystallization drop, incubating for 10 min and flash-cooling in liquid nitrogen before data collection. Data collection and processing: Diffraction data were collected at 100 K on a Rigaku Micromax-003 sealed tube X-ray source and a Dectris Pilatus 200 K detector. The data were indexed, integrated, scaled and merged using xia2 DIALS.<sup>29</sup> Phasing was done by molecular replacement using Phaser<sup>30</sup> and 4JC3 as a starting model and was followed by iterative rounds of refinement and manual model building using Phenix, Refine<sup>31</sup> and Coot,<sup>32</sup> respectively. Model validation was performed using MolProbity.<sup>33</sup> X-ray diffraction data collection and structure refinement statistics are summarized in Table S1. The figures were made using the software PyMol (DeLano Scientific LLC).

**Computational Methods.** Systems preparation. Three-dimensional (3D) coordinates of ternary complexes of (i) 14-3-3ζ/GR/(R)-1; (ii) 14-3-3ζ/GR/(S)-1; (iii) 14-3-3ζ/ERα/(R)-1; and (iv) 14-3-3ζ/ERα/(S)-1 were obtained as follows. 14-3-3ζ/GR/(R)-1 and 14-3-3ζ/GR/(S)-1 were modeled from PDB code 8A9G, which consists of 14-3-3ζ/GR in complex with (R)-18. The 14-3-3ζ/GR's 3D coordinates were extracted from 8A9G, and the binary complex was refined using the Protein Preparation Wizard workflow<sup>34</sup> implemented in Maestro.<sup>35</sup> Hydrogens were added, and charges and protonation states were assigned, titrating the protein at physiological pH. Finally, a minimization step was performed to relieve steric clashes. (R)-1 and (S)-1 were prepared at pH 7.4 ± 1 with LigPrep<sup>36</sup> module implemented in Maestro<sup>35</sup> and subsequently docked on the FC-A pocket using Glide<sup>37</sup> software with default settings in Standard Precision (SP). Three poses were generated for each ligand, and the best-scored pose was used as starting coordinates for the molecular dynamics (MD) simulations (Figure S5). The 14-3-3ζ/ERα binary

complex was modeled using the 14-3-3 $\zeta$ 's 3D coordinates from PDB code 8A9G and ER $\alpha$ 's 3D coordinates from PDB code 6TJM.<sup>8</sup> The complex was submitted to the Protein Preparation Wizard workflow, and (R)-1 and (S)-1 were prepared and docked on the FC-A pocket, as previously described. Also, here, three poses were generated for each ligand, and the best-scored pose was used as starting coordinates for the MD simulations (Figure S5). MD simulations: MD simulations of the four complexes (i.e., 14-3-3 $\zeta$ /GR/(R)-1, 14-3-3 $\zeta$ /GR/(S)-1, 14-3-3 $\zeta$ /ER $\alpha$ /(R)-1, and 14-3-3 $\zeta$ /ER $\alpha$ /(S)-1) were performed with Desmond.<sup>38</sup> Each system was parameterized using the OPLS 2005 force field,<sup>39</sup> embedded in a SCP water box, and neutralized by adding counterions by means of the System Builder module implemented in Maestro.<sup>35</sup> After equilibration performed with default settings, each system was submitted to a production phase of 100 ns in NPT ensemble, using Nosé–Hoover thermostat<sup>40,41</sup> (300 K, relaxation time = 1 ps) and isotropic Martyna–Tobias–Klein barostat<sup>42</sup> (1.01325 bar, relaxation time = 2 ps). Short-range interactions (cutoff = 9 Å) and long-range Coulomb interactions were evaluated using the smooth particle mesh Ewald (PME) method.<sup>43</sup> RESPA integrator was used with a time step of 2 fs. A total of 1000 frames were generated for each trajectory. Simulation Event Analysis module implemented in Maestro was used to monitor distances over the trajectories, and the molecular mechanics/generalized Born surface area (MMGBSA)<sup>44</sup> method was used to estimate the free energy of the binding of (S)-1 and (R)-1.

## ■ ASSOCIATED CONTENT

### SI Supporting Information

The Supporting Information is available free of charge at <https://pubs.acs.org/doi/10.1021/acs.jmedchem.2c01635>.

General procedures; chiral separation and vibrational circular dichroism of **18** and **28**; peptide sequences; 14-3-3 plasmids; fluorescence polarization and surface plasmon resonance assay methods; Caco-2 and GR binding assays; data collection and refinement statistics; crystallographic data of **28**; binding affinity of GR\_pT524 and 14-3-3 in the presence of FC-A; superimposition of crystal structures of GR\_pT524/14-3-3 $\zeta$  and ER $\alpha$ \_pT594/14-3-3 $\sigma$ /FC-A complexes; 14-3-3 $\zeta$ /GR\_pT524 fluorescence polarization assay concentration-response curves of **1–11**; dockings, molecular dynamics simulations and calculated free energy results for **1**; spectroscopic data of products (PDF)  
Molecular formula strings (CSV)

### Accession Codes

14-3-3 $\zeta$ /GR\_pT524/(R)-18 (PDB 8A9G). 14-3-3 $\sigma$ /ER $\alpha$ -(pT594)/(R)-30 (PDB 7PWZ) and 14-3-3 $\sigma$ /ER $\alpha$ (pT594)/(R)-23 (PDB 7PWT). Authors will release the atomic coordinates and experimental data upon article publication.

## ■ AUTHOR INFORMATION

### Corresponding Author

Gavin O'Mahony – Medicinal Chemistry, Research and Early Development, Cardiovascular, Renal and Metabolism, Biopharmaceuticals R&D, AstraZeneca, 43183 Mölndal, Sweden; [orcid.org/0000-0001-5944-1271](https://orcid.org/0000-0001-5944-1271);  
Email: [Gavin.OMahony@astrazeneca.com](mailto:Gavin.OMahony@astrazeneca.com)

### Authors

Jakob S. Pallese – Medicinal Chemistry, Research and Early Development, Cardiovascular, Renal and Metabolism, Biopharmaceuticals R&D, AstraZeneca, 43183 Mölndal, Sweden; [orcid.org/0000-0001-8862-3525](https://orcid.org/0000-0001-8862-3525)  
Claire C. Munier – Medicinal Chemistry, Research and Early Development, Respiratory & Immunology,

Biopharmaceuticals R&D, AstraZeneca, 43183 Mölndal, Sweden; [orcid.org/0000-0002-8517-8398](https://orcid.org/0000-0002-8517-8398)

Francesco Bosica – Medicinal Chemistry, Research and Early Development, Cardiovascular, Renal and Metabolism, Biopharmaceuticals R&D, AstraZeneca, 43183 Mölndal, Sweden

Sebastian A. Andrei – Laboratory of Chemical Biology, Department of Biomedical Engineering and Institute for Complex Molecular Systems, Technische Universiteit Eindhoven, 5612 AZ Eindhoven, The Netherlands

Karl Edman – Discovery Sciences, Biopharmaceuticals R&D, AstraZeneca, 43183 Mölndal, Sweden

Anders Gunnarsson – Discovery Sciences, Biopharmaceuticals R&D, AstraZeneca, 43183 Mölndal, Sweden

Giuseppina La Sala – Medicinal Chemistry, Research and Early Development, Cardiovascular, Renal and Metabolism, Biopharmaceuticals R&D, AstraZeneca, 43183 Mölndal, Sweden; [orcid.org/0000-0001-6565-197X](https://orcid.org/0000-0001-6565-197X)

Okky Dwichandra Putra – Early Product Development and Manufacturing, Pharmaceutical Sciences R&D, AstraZeneca, 43183 Mölndal, Sweden; [orcid.org/0000-0002-6968-1858](https://orcid.org/0000-0002-6968-1858)

Sonja Srdanović – School of Chemistry, Astbury Centre for Structural Molecular Biology, University of Leeds, Leeds, West Yorkshire LS2 9JT, U.K.

Andrew J. Wilson – School of Chemistry, Astbury Centre for Structural Molecular Biology, University of Leeds, Leeds, West Yorkshire LS2 9JT, U.K.; [orcid.org/0000-0001-9852-6366](https://orcid.org/0000-0001-9852-6366)

Lisa Wissler – Discovery Sciences, Biopharmaceuticals R&D, AstraZeneca, 43183 Mölndal, Sweden

Christian Ottmann – Laboratory of Chemical Biology, Department of Biomedical Engineering and Institute for Complex Molecular Systems, Technische Universiteit Eindhoven, 5612 AZ Eindhoven, The Netherlands; [orcid.org/0000-0001-7315-0315](https://orcid.org/0000-0001-7315-0315)

Matthew W. D. Perry – Medicinal Chemistry, Research and Early Development, Respiratory & Immunology, Biopharmaceuticals R&D, AstraZeneca, 43183 Mölndal, Sweden; [orcid.org/0000-0002-9799-0746](https://orcid.org/0000-0002-9799-0746)

Complete contact information is available at:

<https://pubs.acs.org/10.1021/acs.jmedchem.2c01635>

### Author Contributions

<sup>▽</sup>J.S.P. and C.C.M. have contributed equally. The manuscript was written through contributions of all authors.

### Notes

The authors declare no competing financial interest.

C.C.M., K.E., A.G., G.L.S., L.W., M.W.D.P., and G.O'M. are employed by and/or own shares in AstraZeneca. C.O. is a scientific founder of AmbAgon Therapeutics.

## ■ ACKNOWLEDGMENTS

This work was supported by the Initial Training Network TASPPI, funded by the H2020 Marie Curie Actions of the European Commission under Grant Agreement 675179. J.P., C.C.M., and G.O'M. acknowledge Dr. Malin Lemurell, AstraZeneca and the AstraZeneca PostDoc program for their financial support.

## ■ ABBREVIATIONS USED

ACN, acetonitrile; Br, broad; d, doublet; DFT, density functional theory; ER $\alpha$ , estrogen receptor  $\alpha$ ; FA, formic acid; FC-A, fusicoccin A; FP, fluorescence polarization; GR, glucocorticoid receptor; LBD, ligand binding domain; m, multiplet; MMGBSA, molecular mechanics-generalized Born surface area; PPI, protein–protein interaction; q, quartet; RP, reversed-phase; s, singlet; SLS, Swiss Light Source; SPR, surface plasmon resonance; t, triplet

## ■ REFERENCES

- (1) Dong, G.; Ding, Y.; He, S.; Sheng, C. Molecular Glues for Targeted Protein Degradation: From Serendipity to Rational Discovery. *J. Med. Chem.* **2021**, *64*, 10606–10620.
- (2) Békés, M.; Langley, D. R.; Crews, C. M. PROTAC Targeted Protein Degradation: The Past Is Prologue. *Nat. Rev. Drug Discovery* **2022**, *21*, 181–200.
- (3) Munier, C. C.; Ottmann, C.; Perry, M. W. D. 14-3-3 Modulation of the Inflammatory Response. *Pharmacol. Res.* **2021**, *163*, No. 105236.
- (4) Van Der Heide, L. P.; Hoekman, M. F. M.; Smidt, M. P. The Ins and Outs of FoxO Shuttling: Mechanisms of FoxO Translocation and Transcriptional Regulation. *Biochem. J.* **2004**, *380*, 297–309.
- (5) Stevers, L. M.; Wolter, M.; Carlile, G. W.; Macdonald, D.; Richard, L.; Gielen, F.; Hanrahan, J. W.; Thomas, D. Y.; Chakka, S. K.; Peterson, M. L.; Thomas, H.; Brunsveld, L.; Ottmann, C. Macrocyclic-Stabilization of Its Interaction with 14-3-3 Increases Plasma Membrane Localization and Activity of CFTR. *Nat. Commun.* **2022**, *13*, No. 3586.
- (6) Kasahara, K.; Goto, H.; Enomoto, M.; Tomono, Y.; Kiyono, T.; Inagaki, M. 14-3-3 $\gamma$  Mediates Cdc25A Proteolysis to Block Premature Mitotic Entry after DNA Damage. *EMBO J.* **2010**, *29*, 2802–2812.
- (7) Stevers, L. M.; Sijbesma, E.; Botta, M.; Mackintosh, C.; Obsil, T.; Landrieu, I.; Cau, Y.; Wilson, A. J.; Karawajczyk, A.; Eickhoff, J.; Davis, J.; Hann, M.; O'Mahony, G.; Doveston, R. G.; Brunsveld, L.; Ottmann, C. Modulators of 14-3-3 Protein-Protein Interactions. *J. Med. Chem.* **2018**, *61*, 3755–3778.
- (8) Bosica, F.; Andrei, S. A.; Neves, J. F.; Brandt, P.; Gunnarsson, A.; Landrieu, I.; Ottmann, C.; O'Mahony, G. Design of Drug-Like Protein–Protein Interaction Stabilizers Guided by Chelation-Controlled Bioactive Conformation Stabilization. *Chem. - Eur. J.* **2020**, *26*, 7131–7139.
- (9) Smith, B. E.; Wang, S. L.; Jaime-Figueroa, S.; Harbin, A.; Wang, J.; Hamman, B. D.; Crews, C. M. Differential PROTAC Substrate Specificity Dictated by Orientation of Recruited E3 Ligase. *Nat. Commun.* **2019**, *10*, No. 131.
- (10) Kino, T. GR-Regulating Serine/Threonine Kinases: New Physiologic and Pathologic Implications. *Trends Endocrinol. Metab.* **2018**, *29*, 260–270.
- (11) Oakley, R. H.; Cidlowski, J. A. The Biology of the Glucocorticoid Receptor: New Signaling Mechanisms in Health and Disease. *J. Allergy Clin. Immunol.* **2013**, *132*, 1033–1044.
- (12) Weikum, E. R.; Liu, X.; Ortlund, E. A. The Nuclear Receptor Superfamily: A Structural Perspective. *Protein Sci.* **2018**, *27*, 1876–1892.
- (13) Munier, C. C.; De Maria, L.; Edman, K.; Gunnarsson, A.; Longo, M.; MacKintosh, C.; Patel, S.; Snijder, A.; Wissler, L.; Brunsveld, L.; Ottmann, C.; Perry, M. W. D. Glucocorticoid Receptor Thr524 Phosphorylation by MINK1 Induces Interactions with 14-3-3 Protein Regulators. *J. Biol. Chem.* **2021**, *296*, No. 100551.
- (14) Galliher-Beckley, A. J.; Williams, J. G.; Cidlowski, J. A. Ligand-Independent Phosphorylation of the Glucocorticoid Receptor Integrates Cellular Stress Pathways with Nuclear Receptor Signaling. *Mol. Cell. Biol.* **2011**, *31*, 4663–4675.
- (15) Habib, T.; Sadoun, A.; Nader, N.; Suzuki, S.; Liu, W.; Jithesh, P. V.; Kino, T. AKT1 Has Dual Actions on the Glucocorticoid Receptor by Cooperating with 14-3-3. *Mol. Cell. Endocrinol.* **2017**, *439*, 431–443.
- (16) Caratti, B.; Fidan, M.; Caratti, G.; Breitenacker, K.; Engler, M.; Kazemitash, N.; Traut, R.; Wittig, R.; Casanova, E.; Ahmadian, M. R.; Tuckermann, J. P.; Moll, H. P.; Cirstea, I. C. The Glucocorticoid Receptor Associates with RAS Complexes to Inhibit Cell Proliferation and Tumor Growth. *Sci. Signal.* **2022**, *15*, No. eabm4452.
- (17) Zilliacus, J.; Holter, E.; Wakui, H.; Tazawa, H.; Treuter, E.; Gustafsson, J.-Å. Regulation of Glucocorticoid Receptor Activity by 14-3-3-Dependent Intracellular Relocalization of the Corepressor RIP140. *Mol. Endocrinol.* **2001**, *15*, 501–511.
- (18) De Vries-van Leeuwen, I. J.; da Costa Pereira, D.; Flach, K. D.; Piersma, S. R.; Haase, C.; Bier, D.; Yalcin, Z.; Michalides, R.; Feenstra, K. A.; Jiménez, C. R.; de Greef, T. F. A.; Brunsveld, L.; Ottmann, C.; Zwart, W.; de Boer, A. H. Interaction of 14-3-3 Proteins with the Estrogen Receptor Alpha F Domain Provides a Drug Target Interface. *Proc. Natl. Acad. Sci. U.S.A.* **2013**, *110*, 8894–8899.
- (19) Anders, C.; Higuchi, Y.; Koschinsky, K.; Bartel, M.; Schumacher, B.; Thiel, P.; Nitta, H.; Preisig-Müller, R.; Schlichthörl, G.; Renigunta, V.; Ohkanda, J.; Daut, J.; Kato, N.; Ottmann, C. A Semisynthetic Fusicoccane Stabilizes a Protein-Protein Interaction and Enhances the Expression of K<sup>+</sup> Channels at the Cell Surface. *Chem. Biol.* **2013**, *20*, 583–593.
- (20) Ottmann, C.; Weyand, M.; Sassa, T.; Inoue, T.; Kato, N.; Wittinghofer, A.; Oecking, C. A Structural Rationale for Selective Stabilization of Anti-Tumor Interactions of 14-3-3 Proteins by Cotylenin A. *J. Mol. Biol.* **2009**, *386*, 913–919.
- (21) Kappe, C. O. 100 Years of the Biginelli Dihydropyrimidine Synthesis. *Tetrahedron* **1993**, *49*, 6937–6963.
- (22) Nepali, K.; Lee, H. Y.; Liou, J. P. Nitro-Group-Containing Drugs. *J. Med. Chem.* **2019**, *62*, 2851–2893.
- (23) Oprisiu, I.; Winiwarter, S. In Silico ADME Modeling. In *Systems Medicine*; Elsevier B.V., 2021; pp 208–222.
- (24) Fredlund, L.; Winiwarter, S.; Hilgendorf, C. In Vitro Intrinsic Permeability: A Transporter-Independent Measure of Caco-2 Cell Permeability in Drug Design and Development. *Mol. Pharmaceutics* **2017**, *14*, 1601–1609.
- (25) Agilent. CrysAlis PRO. *CrysAlis PRO*; Agilent Technologies Ltd.: Yarnton, England, 2014.
- (26) Sheldrick, G. M. SHELXT - Integrated Space-Group and Crystal-Structure Determination. *Acta Crystallogr., Sect. A: Found. Crystallogr.* **2015**, *71*, 3–8.
- (27) Dolomanov, O. V.; Bourhis, L. J.; Gildea, R. J.; Howard, J. A. K.; Puschmann, H. OLEX2: A Complete Structure Solution, Refinement and Analysis Program. *J. Appl. Crystallogr.* **2009**, *42*, 339–341.
- (28) Sheldrick, G. M. A Short History of SHELX. *Acta Crystallogr., Sect. A: Found. Crystallogr.* **2008**, *64*, 112–122.
- (29) Winter, G. Xia2: An Expert System for Macromolecular Crystallography Data Reduction. *J. Appl. Crystallogr.* **2010**, *43*, 186–190.
- (30) McCoy, A. J. Solving Structures of Protein Complexes by Molecular Replacement with Phaser. *Acta Crystallogr., Sect. D: Biol. Crystallogr.* **2007**, *63*, 32–41.
- (31) Adams, P. D.; Afonine, P. V.; Bunkóczi, G.; Chen, V. B.; Davis, I. W.; Echols, N.; Headd, J. J.; Hung, L. W.; Kapral, G. J.; Grosse-Kunstleve, R. W.; McCoy, A. J.; Moriarty, N. W.; Oeffner, R.; Read, R. J.; Richardson, D. C.; Richardson, J. S.; Terwilliger, T. C.; Zwart, P. H. PHENIX: A Comprehensive Python-Based System for Macromolecular Structure Solution. *Acta Crystallogr., Sect. D: Biol. Crystallogr.* **2010**, *66*, 213–221.
- (32) Emsley, P.; Cowtan, K. Coot: Model-Building Tools for Molecular Graphics. *Acta Crystallogr., Sect. D: Biol. Crystallogr.* **2004**, *60*, 2126–2132.
- (33) Chen, V. B.; Arendall, W. B.; Headd, J. J.; Keedy, D. A.; Immormino, R. M.; Kapral, G. J.; Murray, L. W.; Richardson, J. S.; Richardson, D. C. MolProbity: All-Atom Structure Validation for Macromolecular Crystallography. *Acta Crystallogr., Sect. D: Biol. Crystallogr.* **2010**, *66*, 12–21.

(34) Sastry, G. M.; Adzhigirey, M.; Day, T.; Annabhimoju, R.; Sherman, W. Protein and Ligand Preparation: Parameters, Protocols, and Influence on Virtual Screening Enrichments. *J. Comput. Aided. Mol. Des.* **2013**, *27*, 221–234.

(35) Maestro. *Schrödinger Release 2021–4*; Maestro, Schrödinger, LLC: New York, NY, 2021.

(36) LigPrep. *Schrödinger Release 2021–4*; LigPrep, Schrödinger, LLC: New York, NY, 2021.

(37) Glide. *Schrödinger Release 2021–4*; Glide, Schrödinger, LLC: New York, NY, 2021.

(38) Desmond Molecular Dynamics System. *Schrödinger Release 2021–4*; Maestro-Desmond Interoperability Tools, Schrödinger, 2021.

(39) Shivakumar, D.; Williams, J.; Wu, Y.; Damm, W.; Shelley, J.; Sherman, W. Prediction of Absolute Solvation Free Energies Using Molecular Dynamics Free Energy Perturbation and the Opls Force Field. *J. Chem. Theory Comput.* **2010**, *6*, 1509–1519.

(40) Nosé, S. A Molecular Dynamics Method for Simulations in the Canonical Ensemble. *Mol. Phys.* **1984**, *52*, 255–268.

(41) Hoover, W. G. Canonical Dynamics: Equilibrium Phase-Space Distributions. *Phys. Rev. A* **1985**, *31*, 1695–1697.

(42) Martyna, G. J.; Tobias, D. J.; Klein, M. L. Constant Pressure Molecular Dynamics Algorithms. *J. Chem. Phys.* **1994**, *101*, 4177–4189.

(43) Darden, T.; York, D.; Pedersen, L. Particle Mesh Ewald: An  $N \cdot \log(N)$  Method for Ewald Sums in Large Systems. *J. Chem. Phys.* **1993**, *98*, 10089–10092.

(44) Li, J.; Abel, R.; Zhu, K.; Cao, Y.; Zhao, S.; Friesner, R. A. The VSGB 2.0 Model: A Next Generation Energy Model for High Resolution Protein Structure Modeling. *Proteins* **2011**, *79*, 2794–2812.

## Recommended by ACS

### Discovery and Optimization of *N*-Acyl-6-sulfonamide-tetrahydroquinoline Derivatives as Novel Non-Steroidal Selective Glucocorticoid Receptor Modulators

Dan Li, Tingjun Hou, *et al.*

NOVEMBER 18, 2022  
JOURNAL OF MEDICINAL CHEMISTRY

READ 

### Discovery and Optimization of Potent, Selective, and Brain-Penetrant 1-Heteroaryl-1*H*-Indazole LRRK2 Kinase Inhibitors for the Treatment of Parkinson's Disease

David A. Candito, J. Michael Ellis, *et al.*

DECEMBER 07, 2022  
JOURNAL OF MEDICINAL CHEMISTRY

READ 

### Stereoisomers of an Aryl Pyrazole Glucocorticoid Receptor Agonist Scaffold Elicit Differing Anti-inflammatory Responses

Ashley M. Lato, Shawn R. Campagna, *et al.*

AUGUST 22, 2022  
ACS MEDICINAL CHEMISTRY LETTERS

READ 

### BAY-7081: A Potent, Selective, and Orally Bioavailable Cyanopyridone-Based PDE9A Inhibitor

Daniel Meibom, Frank Wunder, *et al.*

DECEMBER 07, 2022  
JOURNAL OF MEDICINAL CHEMISTRY

READ 

Get More Suggestions >